Emulation of Wind Turbine System using Vector Controlled Induction Motor Drive

Ramu Nair. R, G. Narayanan
Department of Electrical Engineering, Indian Institute of Science, Bangalore, India - 560012
ramun@iisc.ac.in, gnar@iisc.ac.in

***Abstract*—Depleting fossil fuels and concerns about global warming have forced a paradigm shift towards renewable energy resources in meeting our energy requirements. Wind energy utilization has been growing at a rapid rate fuelling research and development in high power wind turbines. To advance research and education in wind energy conversion systems, a controlled test bed is necessary that does not depend on wind availability. In this paper, a control structure is proposed to emulate high power, large inertia wind turbines using low power, small inertia machines. Majority of the existing methods for wind turbine emulation employ DC or induction motors with torque compensation loop. However, it suffers from noise and instability issues. DC motors have several disadvantages compared to induction machines in terms of cost, maintenance, speed and ruggedness, even though their control is simple. Hence, in this paper, Squirrel Cage Induction Machine (SCIM) in speed controlled mode is employed for emulation. The performance of the control structure is demonstrated through an experiment involving step change in wind velocity, where the dynamics of a high inertia wind turbine system are emulated. Simulations and experiments are conducted on a 7.5 *kW* Doubly Fed Induction Generator (DFIG) driven by a 5.5 *kW* SCIM, emulating a wind turbine.**

***Index Terms*—Doubly - fed induction generator, squirrel cage induction motor, vector control, wind turbine, emulation, inertia.**

I. Introduction

The installed wind power capacity is rising rapidly and is anticipated to reach 760 *GW* by 2020 [1]. Major factors for this impressive growth rate are advancements in offshore wind technology, reduction in cost of system components and government incentive programs [1]. Around 50% of the generators employed in wind energy conversion systems are Doubly - Fed Induction Generators (DFIG) [1], [2]. The main factor for the large market share is the reduced power rating of the converters employed for the control of the DFIG, which results in reduced cost and improved efficiency [1]-[3]. A Block diagram of a DFIG based Wind Turbine System (WTS) is shown in Fig. 1. The grid side converter in Fig. 1 performs DC link voltage control, whereas the rotor side converter controls the active and reactive power injection in grid connected mode, and voltage and frequency control in standalone mode. The rotor position information, required by the rotor side current control loops for dq to ABC transformation, can be either sensed or estimated through different sensorless algorithms [1].

This work was supported by CPRI, Ministry of Power, Government of India, under the project *Power conversion, control and protection technologies for microgrid*

Generation of electric power from wind efficiently, reliably and in compliance with modern grid codes demands research and development of advanced control strategies. Wind energy industry is also providing massive job opportunities leading to significant economic development [1]. It is therefore imperative that the operation and control of wind energy conversion systems be taught to engineers to develop skilled man power in the field. Hence, to facilitate research and education, a controlled Test Bed System (TBS) becomes necessary that can emulate high power, large inertia Wind Turbine System (WTS) using low power, small inertia machines, without relying on the availabilty of wind. TBS generally consists of two coupled electric machines: a motor, which acts as the prime mover, and a generator, along with their respective converters for control. Commonly used motors for wind turbine emulation are DC motor or an induction motor. The generator could be DFIG, Permanent Magnet Synchronous Generator (PMSG) or any other generator, as deployed in the field. Although DC motors are favourable from the standpoint of control, they are in general, bulky, expensive and require frequent maintenance due to commutators and brushes. The WTS and the TBS differ basically in two aspects - power level and inertia. The DFIG of the TBS can be operated at the same voltage, current and power levels on a per unit basis, as those of the WTS. Most of the wind turbine emulation schemes reported in literature compensate for the inertia difference between WTS and TBS by controlling the torque of the motor in TBS with a torque compensation loop [3]-[5]. This loop calculates the compensation term by differentiating the speed and hence the loop becomes highly sensitive to noise. Detailed investigations are reported in [3] to show that there are instability issues associated with this approach due to the divergent error component caused by discretisation process in the calculation of acceleration. Torque estimators are employed in [6] for control and emulation of small wind turbines. Hardware in the loop based emulation of variable speed wind turbines can be found in [7].

This work proposes a control structure for emulation of high power, large inertia wind turbines using low power, small inertia induction machines, which are commonly available in a laboratory or industry. The rotor speed (instead of torque) is directly used as the controlled variable for emulating the mechanical dynamics of the WTS on the TBS. With this approach, torque compensation happens by controller action, without the need for an explicit differentiator, thereby avoiding

978-1-5386-9316-2/18/$31.00 ©2018 IEEE

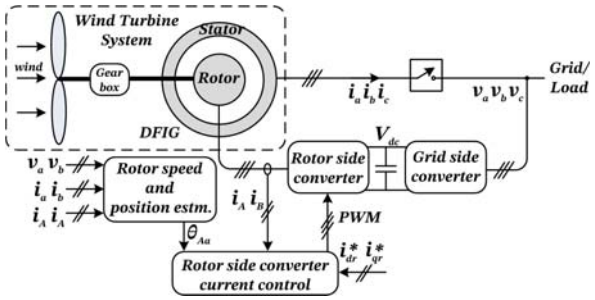

Fig. 1: Control block diagram of DFIG based Wind Turbine System (WTS)

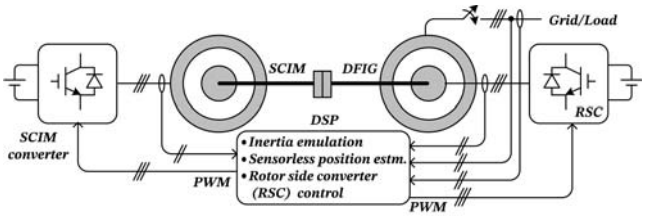

Fig. 2: Control block diagram of Test Bed System (TBS)

noise and instability issues. The control structure is independent of the type or control of the generator, enabling it to be extended to any other generator based WTS.

To begin with, the block diagram of a DFIG based WTS is discussed briefly in section I. Section II describes the requirements for TBS in terms of hardware and control algorithms for the emulation of WTS. The proposed method for emulation of high inertia of WTS on the TBS is explained in detail in section III. It involves estimation of torques of DFIG and wind turbine for generation of reference speed. The actual speed of the TBS is forced to track the reference speed through vector control of SCIM. The speed and current controller designs for vector control are also included in this section. The performance of the control algorithm is demonstrated through an experiment involving step change in wind velocity, where the dynamics of a high inertia WTS are emulated on the TBS. The results of simulations and experiments conducted on a 7.5 *kW* DFIG coupled to a 5.5 *kW* SCIM are given in sections IV and V, respectively. Finally, the paper is concluded in section VI.

II. Test Bed System Description

The TBS configuration is shown in Fig. 2. It consists of an SCIM and a DFIG coupled to the same shaft. These machines are controlled by their respective inverter. The PWM gating pulses for the inverters are generated from a single DSP processor, where three algorithms are implemented - rotor side converter control algorithm, rotor speed and position estimation algorithm and algorithm for emulation of high inertia of WTS on the TBS. The rotor side converter of the DFIG controls the active and reactive power injection in grid connected mode [8], [9], and voltage and frequency control in standalone mode [8]. The rotor speed and position are estimated by rotor current based Model Reference Adaptive Control (MRAC) algorithm [10], by sensing the stator voltages, stator currents and rotor currents of the DFIG. The speed information is required by the proposed method for emulation of high inertia. The rotor side current control loops need rotor position information for dq to ABC transformation. The proposed method for emulation of high inertia of WTS on the TBS is explained in the following section.

III. Proposed Method For Emulation Of High Inertia Of Wind Turbine System

The proposed control structure for emulation of high inertia of WTS on the TBS and the details of controller design are presented in this section.

A. Overall control structure for inertia emulation

The dynamics of speed of a rotational system are determined by inertia and viscous friction of the system and the net torque acting on it. The speed to torque transfer functions of WTS and TBS are indicated in Fig. 3(a) and Fig. 3(b), respectively. In the transfer function, G_{wt}, of WTS, J_{wt} and B_{wt} represent the total inertia and viscous friction, respectively, of various components like wind turbine blades, gear box and generator. Similarly, in the transfer function, G_{tb}, of the TBS, J_{tb} and B_{tb} constitute the combined inertia and viscous friction, respectively, of the SCIM - DFIG set. For the same torque input in *p.u.*, T_{dfig}, if the instantaneous speed of the TBS, ω_{tb} is controlled to be equal to that of the WTS, ω_{wt}, then the TBS emulates the inertia of WTS. The speed to torque transfer function for the speed controlled TBS can be found by block diagram reduction of Fig. 3(c). Feed-forward of DFIG torque reduces the block diagram of Fig. 3(c). The steps for block diagram reduction are shown in Fig. 4. If the bandwidth of the PI controller is high, then ω_{tb} tracks ω_{wt} satisfactorily and the transfer function in Fig. 4(c) can be achieved. The derived transfer function implies that the speed controlled TBS with an inertia of G_{tb} emulates the inertia of WTS, G_{wt}.

B. Reference speed generation

The reference speed for speed control of SCIM is obtained by solving the torque equation of the WTS numerically. Fig. 3(c) shows the block diagram for reference speed generation and the speed control of SCIM with the generated reference speed, ω_{wt}. Numerical solution of torque equation of the WTS requires the estimation of torques of DFIG and the wind turbine blades. The mechanical power of the wind turbine blades, P_{wt}, depends on wind velocity, v_{wind} and coefficient of power, C_p,

$$P_{wt} = \frac{1}{2}\rho A C_p v_{wind}^3 \tag{1}$$

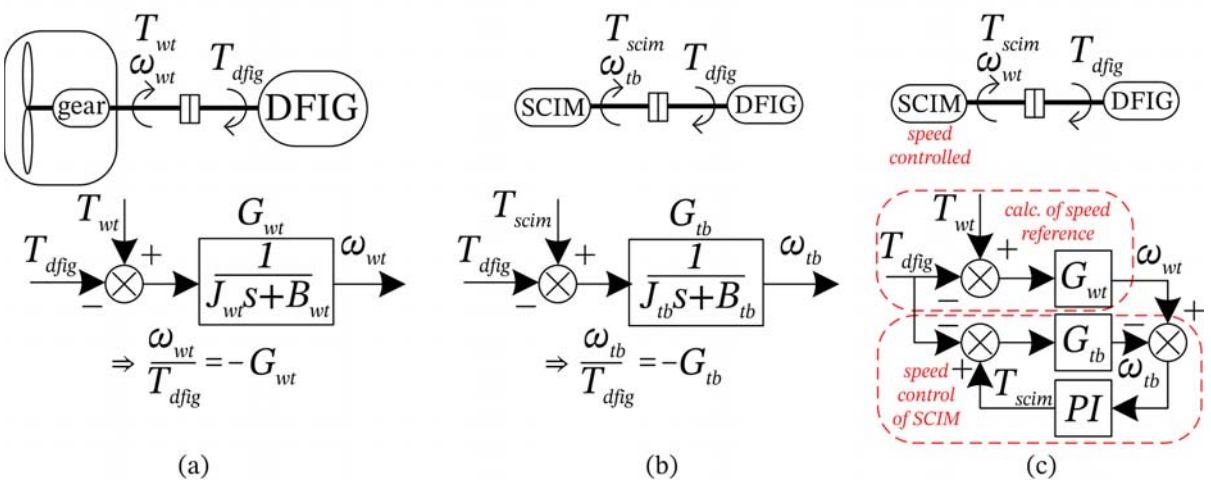

Fig. 3: Speed to torque transfer functions of (a) WTS and (b) TBS without speed control (c) speed controlled TBS

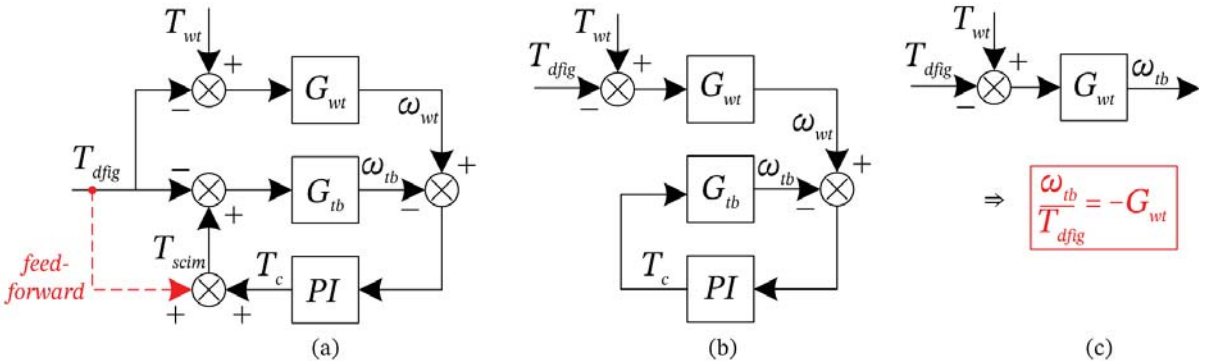

Fig. 4: Block diagram reduction of Fig. 3(c) by feed - forwarding T_{dfig} at the PI output

where, ρ is the air density and A is the area swept by the blades. C_p is a function of tip speed ratio, λ, and pitch angle, β, given by,

$$C_p = c_1(\frac{c_2}{\lambda_i} - c_3\beta - c_4)e^{\frac{-c_5}{\lambda_i}} + c_6\lambda \tag{2}$$

where,

$$\frac{1}{\lambda_i} = \frac{1}{\lambda + 0.08\beta} - \frac{0.035}{\beta^3 + 1} \tag{3}$$

The wind turbine torque, T_{wt}, can be calculated as,

$$T_{wt} = \frac{P_{wt}}{\omega_{wt}} \tag{4}$$

The values of coefficients, c_1 to c_6, and a detailed description on wind turbine modelling can be found in [11]. The DFIG torque can be estimated as,

$$T_{dfig} = \frac{p}{2} n L_m (i_{sq} i_{rd} - i_{sd} i_{rq}) \tag{5}$$

The reference speed, ω_{wt}, can be found by numerical solution of the torque equation as,

$$\omega_n = \omega_{n-1} + (T_{wt} - T_{dfig} - \omega_{n-1} B_{wt}) \frac{T_s}{J_{wt}}, \tag{6}$$

where, T_s is the sampling period.

C. Vector control of SCIM

The speed of the SCIM is forced to track the generated reference speed, ω_{wt} through vector control. Vector control of SCIM involves an outer speed loop which sets the torque reference, T_{scim} and an inner current loop which generates the voltage reference. Note that T_{scim} has to be different from T_{wt} so that ω_{tb} of TBS with low inertia, can track ω_{wt} of WTS, having high inertia. The speed and current controller designs are derived in the following subsection.

1) Speed controller design: The control block diagram for speed controller design is indicated in Fig. 5. The open loop transfer function of the block diagram is given by,

$$G(s) = \frac{(sk_p + k_i)k}{s(J_{tb}s + B_{tb})}, \quad \text{where } k = \frac{p}{2}\frac{L_m^2}{L_r} i_{sd}^* \tag{7}$$

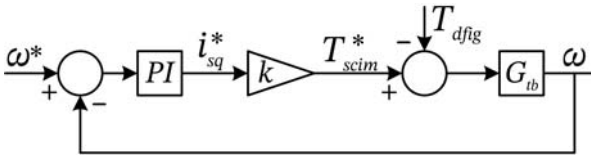

Fig. 5: Block diagram for speed controller design of SCIM

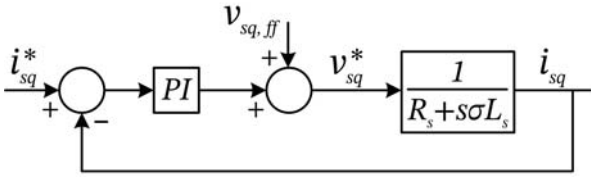

Fig. 6: Block diagram for current controller design of SCIM

At the desired gain crossover frequency, ω_{gc}, the magnitude is unity. Hence,

$$|G(j\omega_{gc})| = \frac{k\sqrt{(\omega_{gc}k_p)^2 + k_i^2}}{\omega_{gc}\sqrt{(\omega_{gc}J_{tb})^2 + B_{tb}^2}} = 1 \tag{8}$$

Further, the phase angle at ω_{gc} should satisfy the phase margin (PM) requirement. Hence,

$$\measuredangle G(j\omega_{gc}) = \tan^{-1}(\frac{\omega_{gc}k_p}{k_i}) - \frac{\pi}{2} - \tan^{-1}(\frac{J_{tb}\omega}{B_{tb}}) \tag{9}$$

$$= -\pi + PM \tag{10}$$

Simultaneous solution of (8) and (10) yields,

$$\frac{k_p}{k_i} = \frac{\tan(PM - \frac{\pi}{2}) + (\frac{J_{tb}\omega_{gc}}{B_{tb}})}{\omega_{gc} - \tan(PM - \frac{\pi}{2})\frac{J_{tb}\omega_{gc}^2}{B_{tb}}} \tag{11}$$

$$k_i = \frac{1}{k}\sqrt{\frac{\omega_{gc}^2(J_{tb}^2\omega_{gc}^2 + B_{tb}^2)}{\omega_{gc}^2(\frac{k_p}{k_i})^2 + 1}} \tag{12}$$

2) Current controller design: The current controller parameters can be designed using Fig. 6. The feed-forward term, $v_{sq,ff}$ in the figure can be evaluated [12] as,

$$v_{sq,ff} = \omega_d\frac{L_m}{L_r}\lambda_{rd} + \omega_d\sigma L_s i_{sd} \tag{13}$$

Following similar approach as in the case of speed controller design, the values of k_p and k_i for current controller can be obtained using,

$$\omega_{gc}\frac{k_p}{k_i} = \tan(PM - \frac{\pi}{2} + \tan^{-1}(\sigma\omega_{gc}\frac{L_s}{R_s})) \tag{14}$$

$$k_i = \omega_{gc}\sqrt{\frac{R_s^2 + (\sigma\omega_{gc}L_s)^2}{1 + (\omega_{gc}\frac{k_p}{k_i})^2}} \tag{15}$$

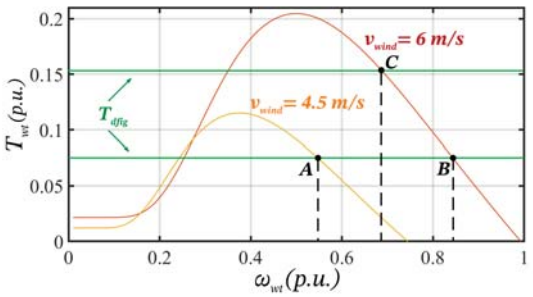

Fig. 7: Wind turbine torque - speed curves

TABLE I: Machine ratings and parameters

Machine	SCIM	DFIG
Power (kW)	5.5	7.5
Voltage (V)	415	400/135
Current (A)	11	15
R_s (Ω)	3	0.77
R_r (Ω)	5	0.16
L_m (mH)	480	230
L_{ls}, L'_{lr} (mH)	20	5
σ	0.0795	0.0581
Turns ratio, n	-	3

IV. Simulation Results

The performance of the control algorithm for emulation of high inertia is first verified through simulations. The parameters of the WTS considered for emulation are $J_{wt} = 100\ kgm^2$ and $B_{wt} = 0.001$ *Nms/rad*. The TBS has $J_{tb} = 0.06\ kgm^2$ and $B_{tb} = 0.005$ *Nms/rad*, as obtained experimentally. The torque - speed characteristics of the WTS are shown in Fig. 7 for two wind speeds. The commanded load voltage and frequency are 120 V and 50 Hz, respectively, on a resistive load of 30 Ω/ph. The control of the DFIG in standalone and grid connected modes are explained in detail in [8]. The rotor side d and q current references are calculated for the commanded voltage and frequency, which are then tracked through respective current controllers. The intersection of T_{dfig} with the torque - speed characteristics of WTS gives the steady state operating point.

The initial steady state operating point is marked as '*A*' in the figure. The dynamic performance of the control structure for a step change in wind velocity from 4.5 *m/s* to 6 *m/s* is simulated. Following step change in wind speed at $t = 40$ s, T_{wt} increases, whereas, T_{dfig} remains constant. This causes the turbine speed, ω_{wt} to increase till it reaches the new steady state, marked as '*B*', where T_{wt} = T_{dfig}. Numerical solution of the torque equation of the WTS yields the turbine speed, which is fed as speed reference to speed controller of SCIM. The output of speed controller is T_{scim}, which changes in such a way that ω_{tb} always tracks ω_{wt}, thus emulating the inertia of WTS on the TBS. As ω_{tb} increases, the rotor excitation frequency, ω_{dA}, decreases, so that their sum, which is the stator

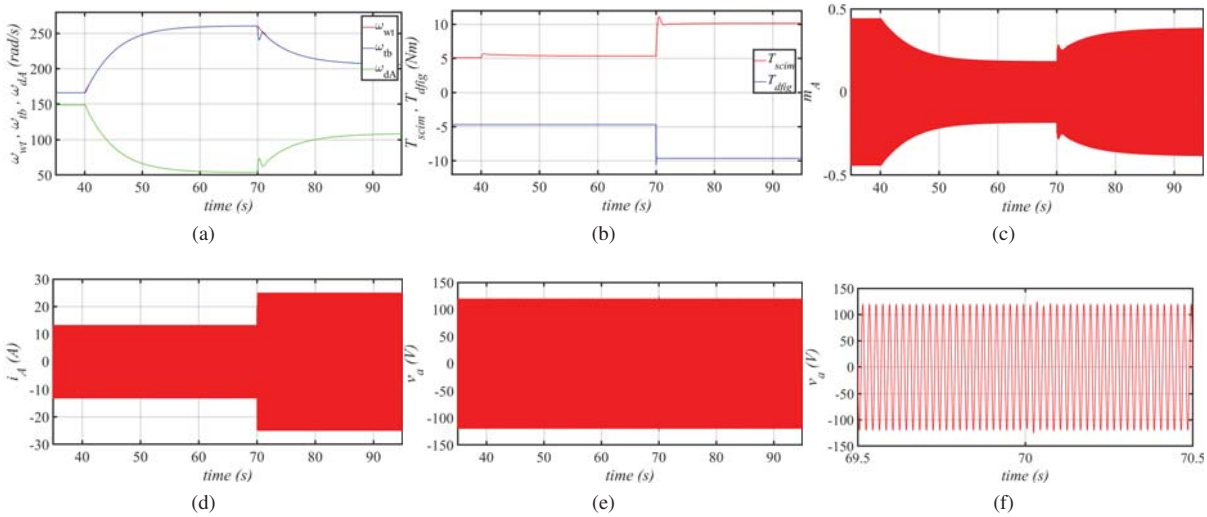

Fig. 8: Simulation results demonstrating the emulation of high inertia of WTS on the TBS, following step change in wind speed and load at $t = 40\ s$ and $t = 70\ s$, respectively. (a) ω_{wt}, ω_{tb}, ω_{dA}, (b) torques of SCIM, T_{scim} and DFIG, T_{dfig}, (c) rotor side modulation index, m_A, (d) rotor side current, i_A, (e) stator voltage, v_a, (f) v_a zoomed

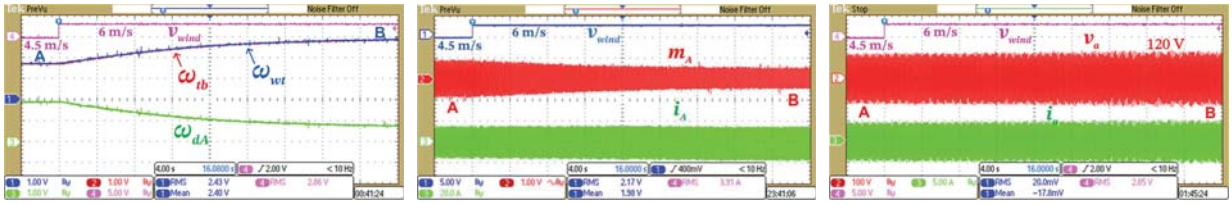

Fig. 9: Experimental results demonstrating the emulation of high inertia of WTS on the TBS, following step change in wind speed. (a) ω_{wt}, ω_{tb}, ω_{dA}, (b) rotor side modulation index, m_A and rotor side current, i_A, (c) stator voltage, v_a and stator current, i_a

side frequency, is maintained at 50 Hz. As ω_{dA} decreases, the voltages required to force the rotor currents reduce, hence the rotor side modulation indices decrease.

After the new steady state at '*B*' is reached, load is increased at $t = 70\ s$. This increases the counter torque of DFIG, thereby decreasing the turbine speed, ω_{wt}. Reduction in ω_{wt} leads to increase in turbine torque, T_{wt}, till it reaches new steady state at '*C*', where $T_{wt} = T_{dfig}$. Irrespective of change in wind speed and load, the voltage on the load is regulated at the commanded value of 120 V. ω_{wt}, ω_{tb}, and ω_{dA} are indicated in Fig. 8(a). Fig. 8(b) shows the torque of the DFIG and SCIM. The modulation index for PWM generation and rotor side current are shown in Figs. 8(c) and 8(d), respectively. The stator side voltage waveform and its zoomed version are presented in Figs. 8(e) and 8(f).

V. Experimental Results

Experiments are conducted on a 7.5 kW DFIG coupled to a 5.5 kW SCIM. The experimental setup is shown in Fig. 10. The parameters and ratings of both the machines are tabulated in Table I. Three control algorithms, as mentioned in section

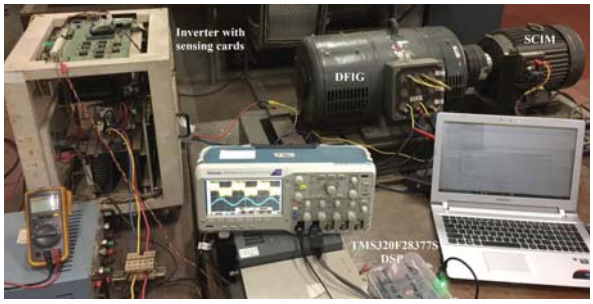

Fig. 10: Experimental setup

II, are implemented in TMS320F28377S DSP. The bandwidths for the speed controller and current controller are 1 Hz and 50 Hz, respectively. Rise time of the speed loop of the SCIM for a step response is 0.5 s. The mechanical time constant of the DFIG - SCIM set is 12 s, as obtained experimentally. A step change in wind speed from 4.5 *m/s* to 6 *m/s* is applied. The dynamics of the different variables in transiting from steady state, '*A*' to steady state, '*B*' are captured in the experimental results. The experimental results show that the high inertia

of WTS is emulated on the TBS, as in simulation results. Fig. 9(a) shows the dynamics of ω_{wt}, ω_{tb} and ω_{dA}. The time taken for the rotor speed to transit from steady state, '*A*' to steady state '*B*' matches closely with the simulation results in Fig. 8(a). The rotor side modulation index, m_A, and rotor side current, i_A, are indicated in Fig. 9(b). These correspond to the simulation results shown in Fig. 8(c) and 8(d), respectively. The stator side voltage, v_a, and stator current, i_a, are shown in Fig. 9(c). The stator voltage is regulated at 120 V at 50 Hz, irrespective of change in wind speed, as in the simulation result in Fig. 8(e).

VI. Conclusion

This paper proposes a control structure for the emulation of high power, large inertia wind turbine system using low power, small inertia induction machines. By tracking the generated reference speed of the WTS, obtained by numerical solution of its torque equation, the desired speed to torque transfer function of WTS is achieved on the TBS. The torque estimations for wind turbine and DFIG are included. The tracking of the reference speed is realised through vector control of the SCIM. The speed and current controller designs for vector control of SCIM are given. The performance of the control algorithm is validated through simulations and experiments, involving step change in wind speed, where the dynamics of WTS with total inertia, J_{wt} = 100 kgm^2 and total viscous friction, B_{wt} = 0.005 *Nms/rad* are emulated.

References

[1] V. Yaramasu, B. Wu, P. C. Sen, S. Kouro and M. Narimani, "High-power wind energy conversion systems: State-of-the-art and emerging technologies," *Proceedings of the IEEE*, vol. 103, no. 5, pp. 740-788, May 2015.

[2] F. Blaabjerg and K. Ma, "Wind energy systems," *Proceedings of the IEEE*, vol. 105, no. 11, pp. 2116-2131, Nov. 2017.

[3] L. Weijie, Y. Minghui, Z. Rui, J. Minghe and Z. Yun, "Investigating instability of the wind turbine simulator with the conventional inertia emulation scheme," *IEEE Energy Conversion Congress and Exposition (ECCE)*, Montreal, QC, pp. 983-989, 2015.

[4] S-H Song, B-C Jeong, H-I Lee, J-J Kim, J-H Oh and G. Venkataramanan, "Emulation of output characteristics of rotor blades using a hardware-in-loop wind turbine simulator," *IEEE Applied Power Electronics Conference (APEC)*, vol. 3. pp. 1791-1796, 2005.

[5] T. Hardy and W. Jewell, "Emulation of a 1.5MW wind turbine with a DC motor," *IEEE Power and Energy Society General Meeting (PESGM)*, Detroit, MI, USA, pp. 1-8, 2011.

[6] J. M. Guerrero, C. Lumbreras, D. D. Reigosa, P. Garcia and F. Briz, "Control and emulation of small wind turbines using torque estimators," *IEEE Trans. on Ind. Appl.*, vol. 53, no. 5, pp. 4863-4876, Sept.-Oct. 2017.

[7] F. Huerta, R. L. Tello and M. Prodanovic, "Real-time power-hardware-in-the-Loop implementation of variable-speed wind turbines," *IEEE Trans. on Ind. Electron.*, vol. 64, no. 3, pp. 1893-1904, March 2017.

[8] R. Cardenas, R. Pena, S. Alepuz and G. M. Asher, "Overview of control systems for the operation of DFIGs in wind energy applications," *IEEE Trans. Ind. Electron.*, vol. 60, no. 7, pp. 2776-2798, July 2013.

[9] H. Tao, H. Ma, Y. Wei, Y. Li and L. Xu, "A novel grid connection method for DFIG based on direct power control," *IEEE Vehicle Power and Propulsion Conference (VPPC)*, Hangzhou, pp. 1-6, 2016.

[10] R. R. Nair and G. Narayanan, "Modified model reference adaptive observer for rotor speed and position estimation in wound rotor induction machine," *IEEE PES Asia-Pacific Power and Energy Engineering Conference (APPEEC)*, Bangalore, pp. 1-6, 2017.

[11] S. Heier, *Grid integration of wind energy*, Chichester: Wiley, 2014.

[12] D. Novotny and T. Lipo, *Vector control and dynamics of AC drives*, Oxford: Clarendon Press, 2005.